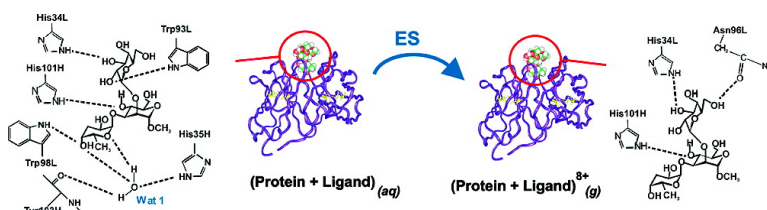Article

Elucidating the Intermolecular Interactions within a Desolvated Protein–Ligand Complex. An Experimental and Computational Study

Elena N. Kitova, Mikyung Seo, Pierre-Nicholas Roy, and John S. Klassen

More About This Article

Additional resources and features associated with this article are available within the HTML version:

- Supporting Information
- Access to high resolution figures
- Links to articles and content related to this article
- Copyright permission to reproduce figures and/or text from this article

View the Full Text HTML

Elucidating the Intermolecular Interactions within a Desolvated Protein−Ligand Complex. An Experimental and Computational Study

Elena N. Kitova, Mikyung Seo, Pierre-Nicholas Roy, and John S. Klassen*

Alberta Ingenuity Centre for Carbohydrate Science and Department of Chemistry, University of Alberta, Edmonton, Alberta, Canada T6G 2G2

Received July 17, 2007; E-mail: john.klassen@ualberta.ca

Abstract: The first detailed study of the intermolecular hydrogens bonds (H-bonds) within a desolvated, noncovalent protein−ligand complex is reported. Using both experimental and computational methods, the intermolecular H-bonds stabilizing protonated and deprotonated ions of a complex composed of a single chain fragment (scFv) of a monoclonal antibody and its native trisaccharide ligand, αGal[αAbe] αMan (**1**), are characterized. Using the blackbody infrared radiative dissociation−functional group replacement (BIRD/ FGR) technique, three H-bond donor−acceptor pairs within the gaseous $(scFv + \mathbf{1})^{n+}$ ions are identified and quantified. Additional sites of interaction on the protein and ligand, for which the binding partner could not be elucidated, are also identified. Comparison of the gas-phase interaction maps with the crystal structure suggests that at least two of the specific H-bonds are conserved upon transfer of the complex from solution to the gas phase by electrospray ionization. However, new (nonspecific) interactions can also form in the gas phase. Notably, the nature and strength of the intermolecular interactions can vary significantly with charge state, and striking differences in the structures of the $(scFv + \mathbf{1})^{n+}$ and $(scFv + \mathbf{1})^{n-}$ ions are evident. Intermolecular H-bonds are also identified from molecular dynamics (MD) simulations performed at the $+8$ and -8 charge states. Agreement is found for a majority of intermolecular interactions predicted for the $(scFv + \mathbf{1})^{8+}$ ion by the MD simulation and BIRD/FGR method; the agreement is less favorable in the case of the $(scFv + \mathbf{1})^{8-}$ ion. However, both the computational and experimental results point to structural differences between the $+8$ and -8 ions. The computational results also provide insights into the structural changes that accompany the loss of interfacial waters from the complex.

Introduction

Most biological processes, including the immune response, cell−cell communication, inflammation, and bacterial and viral infections, involve the association of biomolecules to form specific, noncovalent complexes. The structure and stability of these complexes are determined by the concerted action of many forces (e.g., hydrogen bonds (H-bonds), ionic, and van der Waals interactions) between binding partners and from the displacement and reorganization of solvent molecules associated with the solvent shell of the binding partners. An understanding of these forces, the thermochemistry, and the structures they lead to is essential to a complete understanding of biological processes.

Gas-phase studies of desolvated biological complexes represent a promising experimental approach to probe directly the intrinsic (solute−solute) intermolecular interactions and, indirectly, the role of solvent in biological recognition. The transfer of specific, noncovalent biological complexes from solution to the gas phase is, in most cases, readily achieved using electrospray ionization (ES).[1] Because the interactions between biological macromolecules and individual water molecules are typically weak, the hydration waters are rapidly lost in the gas

phase giving the desolvated ions. Once in the gas phase, the ions can be interrogated using a variety of mass spectrometry (MS)-based techniques.

Elucidating the higher order structures of gaseous ions of large biological molecules and their noncovalent complexes represents a significant experimental challenge. The structures of gaseous biopolymers are normally inferred from ion fragmentation,[2] ion−ion,[3] or ion−molecule reactions[4] or from ion mobility

(1) Loo, J. A. *Mass Spectrom. Rev.* **1997**, *16*, 1−23.

(2) (a) Benesch, J. L. P.; Sobott, F.; Robinson, C. V. *Anal. Chem.* **2003**, *75*, 2208−2214. (b) Loo, J. A.; He, J. X.; Cody, W. L. *J. Am. Chem. Soc.* **1998**, *120*, 4542−4543. (c) Rostom, A. A.; Fucini, P.; Benjamin, D. R.; Juenemann, R.; Nierhaus, K. H.; Hartl, F. U.; Dobson, C. M.; Robinson, C. V. *Proc. Natl. Acad. Sci. U.S.A.* **2000**, *97*, 5185−5190. (d) van Duijn, E.; Simmons, D. A.; van den Heuvel, R. H.; Bakkes, P. J.; van Heerikhuizen, H.; Heeren, R. M.; Robinson, C. V.; van der Vies, S. M.; Heck, A. J. *J. Am. Chem. Soc.* **2006**, *128*, 4694−4702. (e) van den Heuvel, R. H. H.; van Duijn. E.; Mazon, H.; Synowsky, S. A.; Lorenzen, K.; Versluis, C.; Brouns, S. J. J.; Langridge, D.; van der Oost, J.; Hoyes, J.; Heck, A. J. R. *Anal. Chem.* **2006**, *78*, 7473−7483. (f) Wu, Q. Y.; Gao, J. M.; Joseph-McCarthy, D.; Sigal, G. B.; Bruce, J. E.; Whitesides, G. M.; Smith, R. D. *J. Am. Chem. Soc.* **1997**, *119*, 1157−1158. (g) Benesch, J. L. P.; Aquilina, J. A.; Ruotolo, B. T.; Sobott, F.; Robinson, C. V. *Chem. Biol.* **2006**, *13*, 597−605.

(3) (a) Newton, K. A.; Amunugama, R.; McLuckey, S. A. *J. Phys. Chem.* **2005**, *109*, 3608−3616. (b) Zubarev, R. A.; Horn, D. M.; Fridriksson, E. K.; Kelleher, N. L.; Kruger, N. A.; Lewis, M. A.; Carpenter, B. K.; McLafferty, F. W. *Anal. Chem.* **2000**, *72*, 563−573. (c) Breuker, K.; Oh, H. B.; Horn, D. M.; Cerda, B. A.; McLafferty, F. W. *J. Am. Chem. Soc.* **2002**, *124*, 6407−6420. (d) Oh, H.; Breuker, K.; Sze, S. K.; Ge, Y.; Carpenter, B. K.; McLafferty, F. W. *Proc. Natl. Acad. Sci. U.S.A.* **2002**, *99*, 15863−15868.

measurements.[5] More recently, spectroscopic techniques have been applied to gaseous peptides and proteins to evaluate higher order structure.[6,7]

Individual intermolecular interactions within gaseous ions of noncovalent biological complexes are normally inferred from differences in the stability, usually kinetic, of structurally related complexes. For example, the stabilizing role of Watson−Crick hydrogen bonds and base stacking in DNA duplexes in the gas phase have been extensively investigated by dissociation experiments performed on duplexes of varying base composition.[8,9] Douglas and co-workers described the application of collision-induced dissociation combined with functional group modification to evaluate the binding interactions within the gaseous ions of protein−small molecule complexes.[10] Loo and co-workers demonstrated the application of ES-MS and electron capture dissociation to identify the ligand binding site within a desolvated protein−ligand complex.[11]

Recently, our laboratory developed a reactivity-based approach, employing blackbody infrared radiative dissociation (BIRD),[12] a thermal dissociation technique implemented with a Fourier-transform ion cyclotron resonance mass spectrometer (FT-ICR MS), and functional group replacement (FGR) to *identify* individual interactions in gaseous biological complexes and to *quantify* the strength of the interactions.[13] In the BIRD/FGR method, to identify whether a particular functional group, either on the protein or ligand, is involved in binding, the group is modified in such a way that any preexisting interaction is lost. The activation energy, E_a, of the modified complex is then compared to the E_a of the unmodified complex. A decrease in E_a upon modification indicates that the particular functional group stabilized the complex. Furthermore, the difference in E_a, i.e. $\Delta E_a = E_a(\text{unmodified complex}) - E_a(\text{modified complex})$, provides a measure of the strength of the interaction. To identify H-bond donor/acceptor pairs, a *three-step* approach is normally utilized, in which the ΔE_a values are determined for complexes containing a single modification of the ligand (functional group modification), a single modification of the protein (active site mutation), and simultaneous modification of the protein and the ligand (dual modification).[13] For a given donor/acceptor pair,
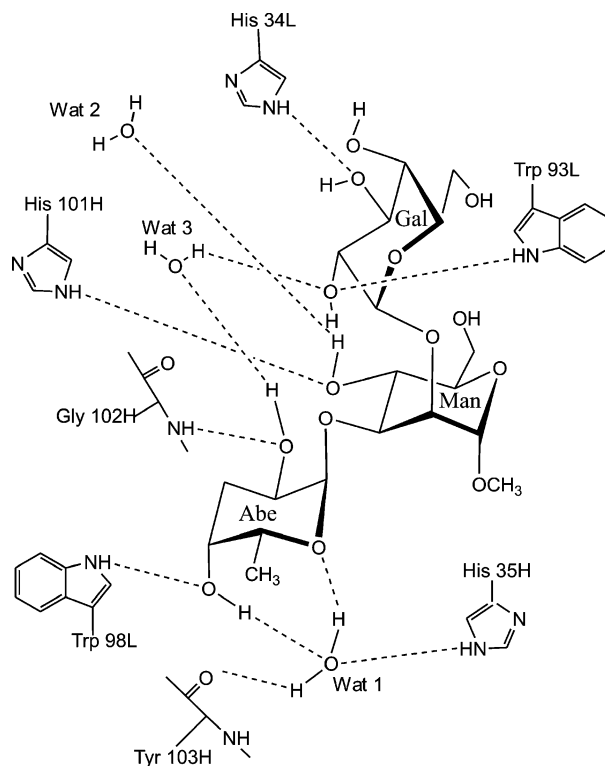

Figure 1. Intermolecular hydrogen bond scheme for the (scFv + **1**) complex obtained from X-ray analysis of the crystal structure.

the magnitude of the ΔE_a values determined for all three complexes will be identical.

In several preliminary studies, our laboratory described the application of the BIRD/FGR technique to a gaseous protein−trisaccharide complex consisting of a genetically engineered single chain variable fragment, scFv, of the monoclonal antibody Se155-4 and its native trisaccharide ligand, αGal[αAbe]αMan (**1**).[13,14] Crystal structures for the (scFv + **1**) complex[15a] and the corresponding antigen binding fragment (Fab) complex have been solved. Analysis of the crystal structures suggests that **1** is bound to the scFv through as many as five intermolecular H-bonds in solution (Figure 1). Additionally, a water molecule (Wat1) at the base of the binding site, which mediates H-bonds between scFv and **1**, has been identified. Two additional waters (Wat2, Wat3) are also observed in the crystal structures. Our laboratory has previously shown that one of the specific intermolecular H-bonds (His[101H]−Man C4 OH) is preserved in the gas phase, at least at certain charge states.[13b,14] Indirect evidence for the formation of nonspecific interactions, i.e., interactions not present in solution but which form in the gas phase, was also reported.[13a] Here, we seek to provide a complete description of the intermolecular interactions within the protonated and deprotonated ions of the desolvated (scFv + **1**) complex. With this objective in mind, the BIRD/FGR technique was applied to the complexes of **1** and monodeoxy analogues thereof, with the scFv and an array of single point scFv mutants. Measurements were performed over a range of charge states in order to assess the influence of charge on the nature and strength

(4) (a) McLafferty, F. W.; Guan, Z. Q.; Haupts, U.; Wood, T. D.; Kelleher, N. L. *J. Am. Chem. Soc.* **1998**, *120*, 4732−4740. (b) Gross, D. S.; Schnier, P. D.; Rodriguez-Cruz, S. E.; Fagerquist, C. K.; Williams, E. R. *Proc. Natl. Acad. Sci. U.S.A.* **2002**, *93*, 3143−3148.
(5) (a) Shelimov, K. B.; Clemmer, D. E.; Hudgins, R. R.; Jarrold, M. F. *J. Am. Chem. Soc.* **1997**, *119*, 2240−2248. (b) Robinson, E. W.; Leib, R. D.; Williams, E. R. *J. Am. Soc. Mass Spectrom.* **2006**, *17*, 1469−1479. (c) Koeniger, S. L.; Merenbloom, S. I.; Sevugarajan, S.; Clemmer, D. E. *J. Am. Chem. Soc.* **2006**, *128*, 11713−11719. (d) Ruotolo, B. T.; Giles, K.; Campuzano, I.; Sandercock, A. M.; Bateman, R. H.; Robinson, C. V. *Science* **2005**, *310*, 1658−1661.
(6) (a) Oomens, J.; Polfer, N.; Moore, D. T.; van der Meer, L.; Marshall, A. G.; Eyler, J. R.; Meijer, G.; von Helden, G. *Phys. Chem. Chem. Phys.* **2005**, *7*, 1345−1348. (b) Compagnon, I.; Oomens, J.; Meijer, G.; von Helden, G. *J. Am. Chem. Soc.* **2006**, *128*, 3592−3597.
(7) Iavarone, A. T.; Parks, J. H. *J. Am. Chem. Soc.* **2005**, *127*, 8606−8607.
(8) Schnier, P. D.; Klassen, J. S.; Strittmatter, E. E.; Williams, E. R. *J. Am. Chem. Soc.* **1998**, *120*, 9605−9613.
(9) (a) Gabelica, V.; De Pauw, E. *J. Mass Spectrom.* **2001**, *36*, 397−402. (b) Gabelica, V.; De Pauw, E. *J. Am. Soc. Mass Spectrom.* **2002**, *13*, 91−98. (c) Gabelica, V.; De Pauw, E. *Int. J. Mass Spectrom.* **2002**, *219*, 151−159.
(10) Tešić, M.; Wicki, J.; Poon, D. K. Y.; Withers, S. G.; Douglas, D. J. *J. Am. Soc. Mass Spectrom.* **2007**, *18*, 64−73.
(11) Xie, Y.; Zhang, J.; Yin, S.; Loo, J. A. *J. Am. Chem. Soc.* **2006**, *128*, 14432−14433.
(12) (a) Dunbar, R. C.; McMahon, T. B. *Science* **1998**, *279*, 194−197. (b) Price, W. D.; Schnier, P. D.; Jockush, R. A.; Strittmatter, E. F.; Williams, E. R. *J. Am. Chem. Soc.* **1996**, *118*, 10640−10644.
(13) (a) Kitova, E. N.; Bundle, D. R.; Klassen, J. S. *J. Am. Chem. Soc.* **2002**, *124*, 5902−5913. (b) Kitova, E. N.; Bundle, D. R.; Klassen, J. S. *Angew. Chem., Int. Ed.* **2004**, *43*, 4183−4186.
(14) Kitova, E. N.; Bundle, D. R.; Klassen, J. S. *J. Am. Chem. Soc.* **2002**, *124*, 9340−9341.
(15) (a) Zdanov, A.; Bundle, D. R.; Deng, S.-J.; MacKenzie, C. R.; Narang, S. A.; Young, M. N.; Cygler, M. *Proc. Natl. Acad. Sci. U.S.A.* **1994**, *91*, 6423−6427. (b) Bundle, D. R.; Baumann, H.; Brisson, J. R.; Gagne, S. M.; Zdanov, A.; Cygler, M. *Biochemistry* **1994**, *33*, 5183−5192.

of the intermolecular interactions. To complement the gas phase measurements, molecular dynamics (MD) simulations were performed on the gaseous (scFv + **1**)$^{+8}$ and (scFv + **1**)$^{-8}$ ions and the intermolecular H-bonds were identified. Taken together, the results of this study provide the first detailed and quantitative description of the intermolecular interactions within the gaseous ions of a protein−ligand complex. Comparison of the interactions identified in the gas phase with the H-bond map inferred from crystallographic data provides new insights into the structural changes that accompany the transfer of protein−ligand complexes from solution to the gas phase by ES and the influence of charge state thereon.

Experimental Section

Proteins and Ligands. The recombinant scFv protein (MW 26 539 Da) of the monoclonal antibody Se155-4 was expressed in *E. coli* and isolated and purified using a procedure which was described previously.[15] Using site-directed mutagenesis, a series of single-point mutants were prepared: His[101H]Ala, His[101H]Arg, His[101H]Lys, His[101H]Gln, His[34L]-Ala, His[35H]Ala, His[97L]Ala, Trp[33H]Ala, Trp[93L]Ala, Trp[98L]Ala, Asn[96L]Ala. The designation L and H correspond to the variable regions of the light and the heavy chains of the monoclonal antibody, respectively. Of these mutants, the Trp[33H]Ala, Trp[93L]Ala, Trp[98L]Ala mutants could not be isolated in sufficient yield using the standard affinity purification method. To overcome the difficulty with purification, a polyhistidine segment (a 13 residue myc epitope tag followed by 5 histidines at the C-terminus) was incorporated into the protein. The His-tagged scFv mutants (scFv$_{His}$) were successfully isolated using Ni-NTA Superflow resin. The synthetic trisaccharide ligands (L) used in this study, αGal-[αAbe]αMan (**1**), (3-deoxyαGal)[αAbe]αMan (**2**), (6-deoxyαGal)-[αAbe]αMan (**3**) αGal[αAbe](4-deoxyαMan) (**4**) and αGal[αAbe](6-deoxyαMan) (**5**), were donated by D. Bundle (University of Alberta). The structures of the carbohydrate ligands are shown in Figure 2. Protein stock solutions were prepared at a concentration of 100 μM in 50 mM aqueous ammonium acetate (pH 7). Aqueous stock solutions of the trisaccharide ligands were prepared at a concentration of 1 mM. ES solutions containing L (5−20 μM) and protein (5−10 μM) in 10 mM aqueous ammonium acetate (pH 7) were prepared from the stock solutions. Where a reduction of charge state for the gaseous (scFv + L)$^{n+/-}$ ions was desired, imidazole (100 μM) was added to the ES solution.

Mass Spectrometry. Mass spectra were obtained using an ApexII Fourier-transform ion cyclotron resonance (FT-ICR) mass spectrometer (Bruker, Billerica MA) equipped with a 4.7 or 9.4 T superconducting magnet and an external ES ion source. Nanoflow ES (nanoES) was performed using an aluminosilicate capillary (0.68 mm i.d.) pulled to approximately 4−7 μm o.d. at one end using a micropipette puller (Sutter Instrument Co., Novato, CA). The electric field required to spray the solution was established by applying a voltage of 800 to1000 V in positive ion mode and −600 to −800 V in negative ion mode to a platinum wire inserted inside the glass tip. The solution flow rate ranged from approximately 5 to 50 nL/min depending on the dimensions of the nanoES tip and the applied voltage. The droplets and gaseous ions produced by ES were introduced into the vacuum chamber of mass spectrometer through a stainless steel capillary (i.d. 0.42 mm) maintained at an external temperature of 66 °C. The ion/gas jet sampled by the capillary (±52 V) was transmitted through a skimmer (±4 V) and stored, electrodynamically, in a rf hexapole. Ions were accumulated in the hexapole for 2−5 s, depending on the signal intensity, and then ejected and accelerated (∼±2700 V) into the superconducting magnet, decelerated, and introduced into the ion cell. The trapping plates of the cell were maintained at a constant potential of ±1.3 V throughout the experiments. The typical base pressure for the instrument was ∼5 × 10^{-10} mbar. The temperature of the ion cell was controlled with two
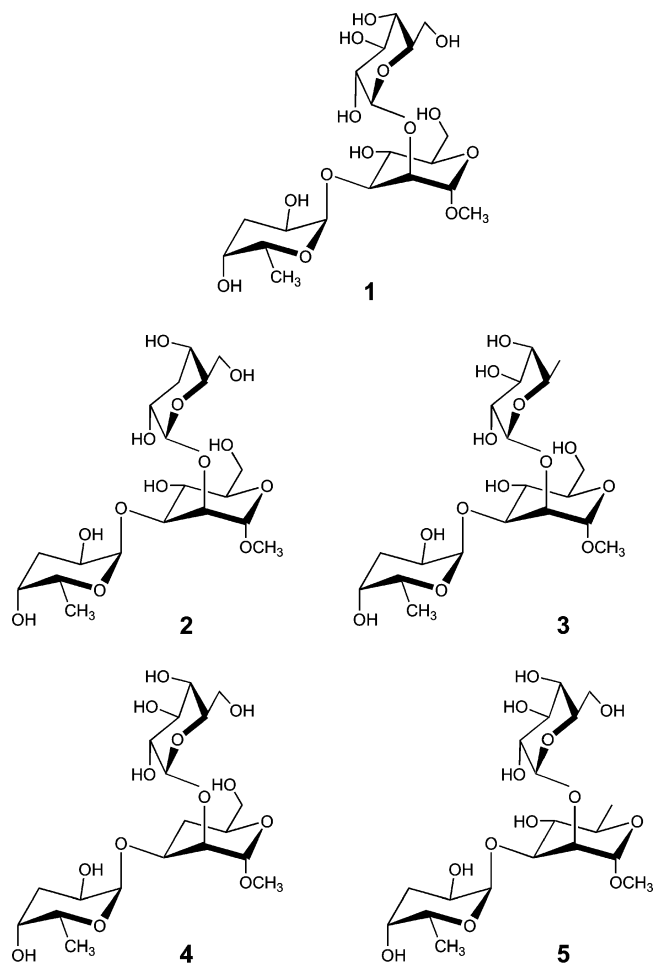
Figure 2. Structures of the trisaccharide ligands, αGal[αAbe]αMan (**1**), (3-deoxyαGal)[αAbe]αMan (**2**), (6-deoxyαGal)[αAbe]αMan (**3**), αGal-[αAbe](4-deoxyαMan) (**4**), and αGal[αAbe](6-deoxyαMan) (**5**).

external flexible heating blankets placed around the vacuum tube in the vicinity of the cell.[16]

Data acquisition was controlled by an SGI R5000 computer running the Bruker Daltonics XMASS software, version 5.0. Mass spectra were obtained using standard experimental sequences with chirp broadband excitation. Isolation of the parent ions for the BIRD experiments was achieved using single rf frequency and broadband rf sweep excitation. The isolated ions were stored inside the heated cell for variable reaction times prior to excitation and detection. The excitation pulse length was 12 μs, and the power of excitation pulse was varied so as to maximize the intensity of the ion signal. The time-domain signal, consisting of the sum of 30 transients containing 128 K data points per transient, was subjected to one zero-fill prior to Fourier-transformation.

Computational Methods. MD simulations were performed using the AMBER 9.0 program suite.[17] The crystal structure (1MFA)[15a] was used for the initial geometry of the (scFv + **1**) complex. The simulations were performed using the AMBER 94 forcefield with the GLYCAM parameter set for oligosaccharides.[18] Currently with AMBER, atomic charges and (atom type) parameters are only available for the Arg residue in its protonated form. Consequently, it was necessary to develop charges and parameters for the neutral form of Arg. These will be described in a forthcoming publication.[19] Electrostatic potential (ESP)

(16) Felitsyn, N.; Kitova, E. N.; Klassen, J. S. *Anal. Chem.* **2001**, *73*, 4647−4661.
(17) Case, D. A. et al. AMBER 9, University of California, San Francisco, 2006.
(18) Woods, R. J.; Dwek, R. J.; Edge, C. J.; Frase-Reid, B. *J. Phys. Chem.* **1995**, *99*, 3832−3846.
(19) Greene, K.; Seo, M.; Brown, A.; Roy, P.-N. Manuscript in preparation.

atomic partial charges, determined by Woods and co-workers,[20] were used for **1**. The (scFv + **1**) complex at the +8 and −8 charge states were chosen for investigation. As described in more detail below, ten different charge distributions were considered for each charge state. The energies of the desolvated (scFv + **1**)$^{8+/−}$ ions were first minimized with the conjugate gradient method using a 0.0001 kcal/mol Å convergence criterion. Each ion was then heated from 10 to 300 K over a period of 15 ps. In order to mimic experimental conditions, simulations were performed in the gas phase under isothermal conditions. Constant temperature was maintained using the weak-coupling algorithm with time constant 1.0 ps.[21] During the simulation, bond length constraints were applied to all hydrogen-containing bonds using the SHAKE algorithm.[22] The system was equilibrated for 1 ns with a time step of 1 fs. After this period, production dynamics were performed for 4 ns and data were collected every 500 fs. Upon completion of the simulations, analysis of structural parameters was carried out: the C_α root-mean-square deviation (rmsd) for scFv, the OH oxygen rmsd for **1**, the dihedral angles associated with the glycosidic linkages in **1** and the intermolecular H-bonds. The geometric criteria used to establish H-bonds are heavy atom (A) to heavy atom (B) distance (r) ≤ 4.0 Å and AHB bond angle ≥120°. Additionally, the occupancy, i.e., the fraction (f) of the simulation steps for which the H-bond criteria are satisfied, was evaluated.

Results and Discussion

Formation of Gaseous (scFv + L)$^{n+/−}$ Ions. Gaseous (scFv + **1**)$^{n+/−}$ ions with a broad range of charge states, both in positive and negative ion mode, were produced by ES. In positive ion mode, ES performed on aqueous solutions of scFv and **1** at solution flow rates of between 20 and 50 nL/min led predominantly to the observation of protonated protein ions, (scFv + nH)$^{n+}$ ≡ scFv^{n+}, and the 1:1 complex ions, (scFv + **1** +nH)$^{n+}$ ≡ (scFv + **1**)$^{n+}$, ions at charge states n = 9−11 (Figure 3a). From the expanded portion of the mass spectrum shown in Figure 3a, it can be seen that there are two peaks corresponding to scFv ions. The peak at higher mass-to-charge ratio (m/z) coincides with the expected mass of the scFv, based on the DNA sequence of the plasmid used to express the protein in *E. coli*. The second peak corresponds to a modified form of the scFv, which has a molecular weight that is 18 Da lower.[23] In addition to the protonated species, ions containing one or more alkali metal ions, Na$^+$ or K$^+$, are also commonly observed, albeit at low abundance. At lower solution flow rates, <20 nL/min, only the fully protonated scFv^{n+} and (scFv + **1**)$^{n+}$ ions were observed, at charge states n = 10−14 (Figure 3b). It is possible to access lower charge states by adding imidazole (∼100 μM) to the ES solution. Imidazole has a relatively high gas-phase basicity (GB = 217 kcal/mol)[24] and is able to effect proton transfer from the scFv^{n+} and (scFv + **1**)$^{n+}$ ions (Figure 3c).

In negative ion mode, ES performed on aqueous solutions of scFv and **1** resulted predominantly in the deprotonated (scFv − nH)$^{n−}$ ≡ scFv$^{n−}$ and (scFv + **1** − nH)$^{n−}$ ≡ (scFv + **1**)$^{n−}$ ions, at n = 7−9 (Figure 3d). Adducts corresponding to the attachment of the acids, CH$_3$COOH (HAc), HCl, and H$_3$PO$_4$, were also observed. The addition of imidazole to the solution in negative ion mode resulted in a decrease in the observed
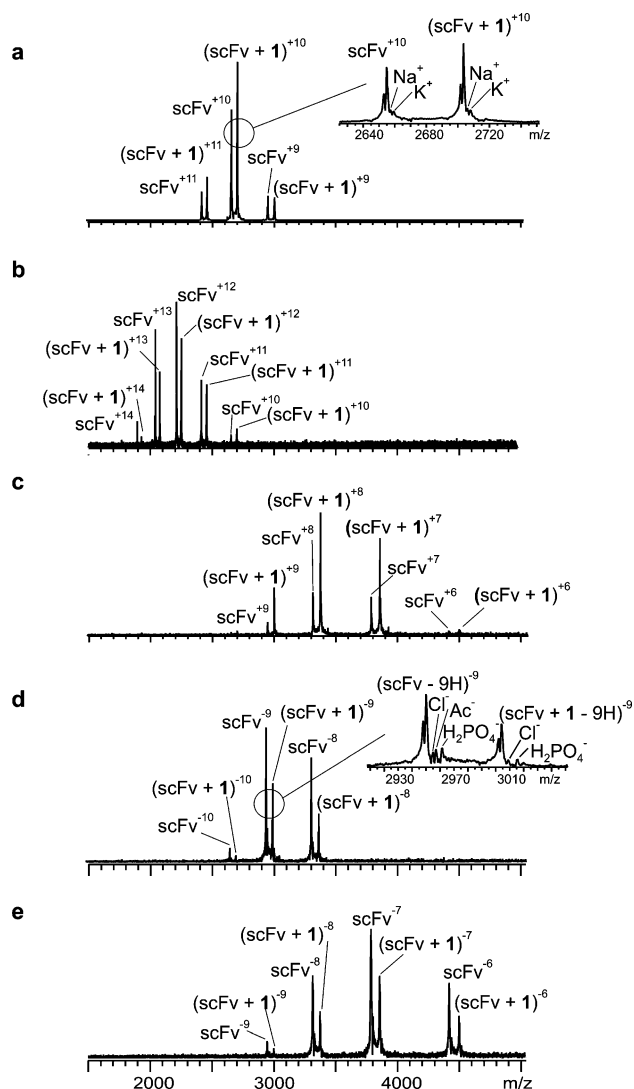

Figure 3. Illustrative nanoES mass spectra of an aqueous solution of 5−10 μM scFv and 5−20 μM **1** in 10 mM ammonium acetate (pH 7) obtained in positive mode: (a) high solution flow rate (∼50 μL/min), (b) low flow rate (∼5 μL/min), or (c) in presence of 100 mM imidazole; and in negative mode: (d) high flow rate (∼50 μL/min), or (e) in presence of 100 mM imidazole.

charge state. This reflects the relatively low gas phase acidity of imidazole (GA = 343 kcal/mol)[25] and its ability to transfer its proton to the deprotonated scFv$^{n−}$ and (scFv + **1**)$^{n−}$ ions (Figure 3e).

It should be noted that there was no evidence for the retention of the interfacial water molecules, which are observed in the (scFv + **1**) and (Fab + **1**) crystal structures, in any of the gaseous (scFv + **1**)$^{n+/−}$ ions. The kinetic stabilities of these interfacial waters are, presumably, similar to the waters that constitute the inner hydration layer of the complex and which are rapidly lost in the gas phase.

Using the procedures described above, gaseous protonated and deprotonated ions of the (scFv + L) complexes composed of the mutant scFv proteins with L = **1−5** and scFv with L = **2−5,** at the same range of charge states as observed for the (scFv + **1**)$^{n+/−}$ ions, were produced. Notably, gaseous ions of the (scFv$_{His}$ + L) complexes composed of the mutants, Trp^{33H}-

(20) Pathiaseril, A.; Woods, R. J. *J. Am. Chem. Soc.* **2000**, *122*, 331−338.
(21) Berndsen, H. J. C.; Postma, J. P. M.; Vangunsteren, W. F.; Dinola, A.; Haak, J. R. *J. Chem. Phys.* **1984**, *81*, 3684−3690.
(22) Ryckaert, J.-P.; Ciccotti, G.; Berendsen, H. J. C. *J. Comput. Phys.* **1977**, *23*, 327−341.
(23) Wang, W. J.; Kitova, E. N.; Klassen, J. S. *Anal. Chem.* **2003**, *75*, 4945−4955.
(24) Hunter, E. P.; Lias, S. G. *Phys. Chem. Ref. Data* **1998**, *27* (3), 413−656.

(25) Taft, R. W.; Anvia, F.; Taagepera, M.; Catalan, J.; Elguero, J. *J. Am. Chem. Soc.* **1986**, *108*, 3237−3239.
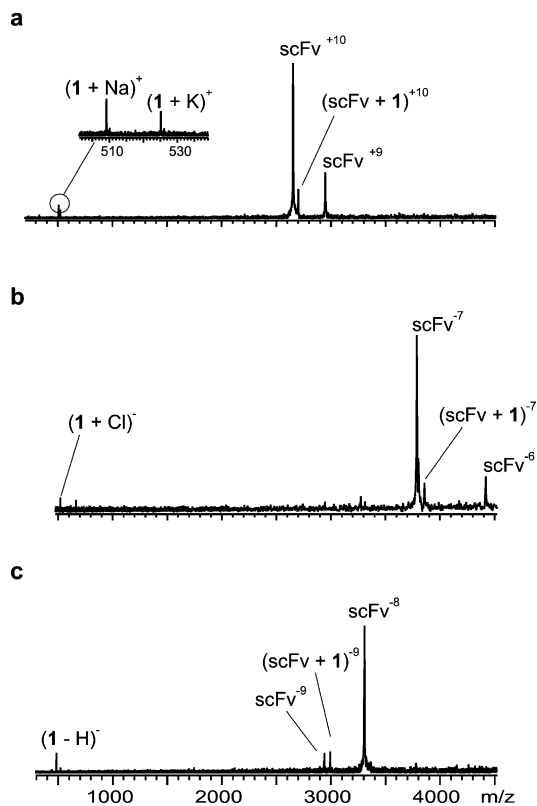
Figure 4. BIRD mass spectra obtained for protonated and deprotonated $(scFv + 1)^{n+/-}$ ions (a) $n = +10$, 154 °C, 6 s; (b) $n = -8$, 147 °C, 5 s; (c) $n = -9$, 147 °C, 5 s.
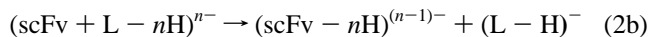
Ala, Trp^{93L}Ala, and Trp^{98L}Ala, could not be detected. Their absence likely reflects a substantial loss of ligand binding in solution because of conformational changes in the scFv upon mutation of the Trp residues.

Dissociation Pathways of the $(scFv + L)^{n+/-}$ Ions. BIRD was performed on the protonated and deprotonated $(scFv + L)^{n+/-}$ ions at charge states +6 to +13 and −6 to −9. At reaction temperatures of between 100 and 180 °C, the only reaction observed for the protonated complexes was the dissociation of the noncovalent intermolecular interactions leading to the loss of the neutral L, eq 1.

$$(scFv + L + nH)^{n+} \rightarrow (scFv + nH)^{n+} + L \qquad (1)$$

The $(scFv + L)^{n+}$ ions containing Na$^+$ and K$^+$ adducts dissociate predominantly by the loss of charged L, as the $(L + Na)^+$ and $(L + K)^+$ ions. Shown in Figure 4a is an illustrative BIRD mass spectrum obtained for the $(scFv + 1)^{+10}$ ion.

BIRD of the deprotonated complexes was found to proceed either by the loss of neutral or deprotonated L, eq 2a,b:

$$(scFv + L - nH)^{n-} \rightarrow (scFv - nH)^{n-} + L \qquad (2a)$$

$$(scFv + L - nH)^{n-} \rightarrow (scFv - nH)^{(n-1)-} + (L - H)^- \qquad (2b)$$

The dominant dissociation pathway depends on the charge state of the complex. At charge states −10 and higher (i.e., −11, −12,...), dissociation occurs exclusively by the loss of deprotonated L, while at charge states −6 to −8, dissociation occurs exclusively by the loss of neutral L (Figure 4b). At charge state −9, both pathways were found to operate (Figure 4c). The loss of deprotonated L can be explained by the low intrinsic GA of

carbohydrates. For example, the GA of glucose has been determined to be between 328 and 336 kcal/mol.[26] In contrast, the GAs of the carboxylic acid side chains of Asp and Glu are expected to be ~240 kcal/mol.[27] Although the GAs of **1−5** have not been determined, they are likely to be similar (or lower) to that of glucose. Consequently, the trisccharides are expected to be able to compete with the acidic amino acid residues of the scFv for the negative charge, particularly at the more negative charge states.

Dissociation Kinetics and Arrhenius Parameters. Rate constants for the loss of neutral L from the protonated and deprotonated $(scFv + L)^{n+/-}$ ions were determined from a linear least-squares fit of plots of the natural logarithm of the relative abundance (A_R) of the complex versus reaction time. The value of A_R was calculated using eq 3:

$$A_R = I_{scFvL}/(I_{scFvL} + I_{scFv}) \qquad (3)$$

where I_{scFvL} and I_{scFv} are the measured intensities of the $(scFv + L)^{n+/-}$ and $scFv^{n+/-}$ ions, respectively. Illustrative kinetic plots, obtained for the dissociation of the $(scFv + 1)^{+7}$, $(scFv + 1)^{+12}$, and $(scFv + 1)^{-8}$ ions, are shown in Figure 5. The kinetic plots exhibit good linearity with near-zero intercepts at the temperatures investigated. Plots of similar quality were obtained for all of the complexes at all of the charge states investigated. This kinetic behavior is consistent with a single dominant complex structure at each charge state or multiple, rapidly interconverting structures. It is interesting to note that Clemmer and co-workers recently reported evidence for many, nonconverting structures for gaseous protein ions at a given charge state.[28] The present results indicate that, if multiple, nonconverting complex structures for the $(scFv + L)^{n+/-}$ ions do indeed exist, they exhibit identical dissociation kinetics.

Shown in Figure 6 are Arrhenius plots constructed from the temperature-dependent rate constants measured for the loss of **1** from the protonated (Figure 6a) and deprotonated $(scFv + 1)^{n+/-}$ (Figure 6b) ions. Arrhenius plots for the $(scFv + L)^{n+/-}$ ions of the structurally modified complexes composed of the scFv mutants and monodeoxy ligands are given as Supporting Information (SI). For each ion, the value of E_a was determined from the slope of the linear least-squares fit of the Arrhenius plot and the preexponential (A) factor was determined from the y-intercept of the fit. The Arrhenius parameters for the dissociation of all of the protonated and deprotonated ions are listed in Tables 1 and 2.

Influence of Charge State on the Stability of the $(scFv + 1)^{n+/-}$ Ions. Inspection of the Arrhenius plots shown in Figure 6 and SI reveals that the kinetic stabilities of the $(scFv + L)^{n+/-}$ ions are sensitive to charge state. For the $(scFv + 1)^{n+}$ ions, the +8 and +9 ions are found to be the most stable (kinetically) over the temperature range investigated; the kinetic stability decreasing at both higher and lower charge states. The dissociation rate constants measured for the deprotonated $(scFv + 1)^{n-}$ ions, at $n = 6$ to 8, are similar and are intermediate to those determined for the +8/+9 and +10 ions (at the temperatures investigated). Although exceptions exist, a similar trend

(26) Salpin, J. Y.; Tortajada, J. *J. Mass Spectrom.* **2004**, *39*, 930−941.
(27) (a) In *Gas-Phase Ion Chemistry*; Bowers, M. T., Ed.; Academic Press: New York, 1979; Vol. 2, Chapter 11. (b) Cumming, J. B.; Kebarle, P. *Can. J. Chem.* **1978**, *56*, 1−9.
(28) Koeniger, S. L.; Merenbloom, S. I.; Clemmer, D. E. *J. Phys. Chem. B* **2006**, *110*, 7017−7021.
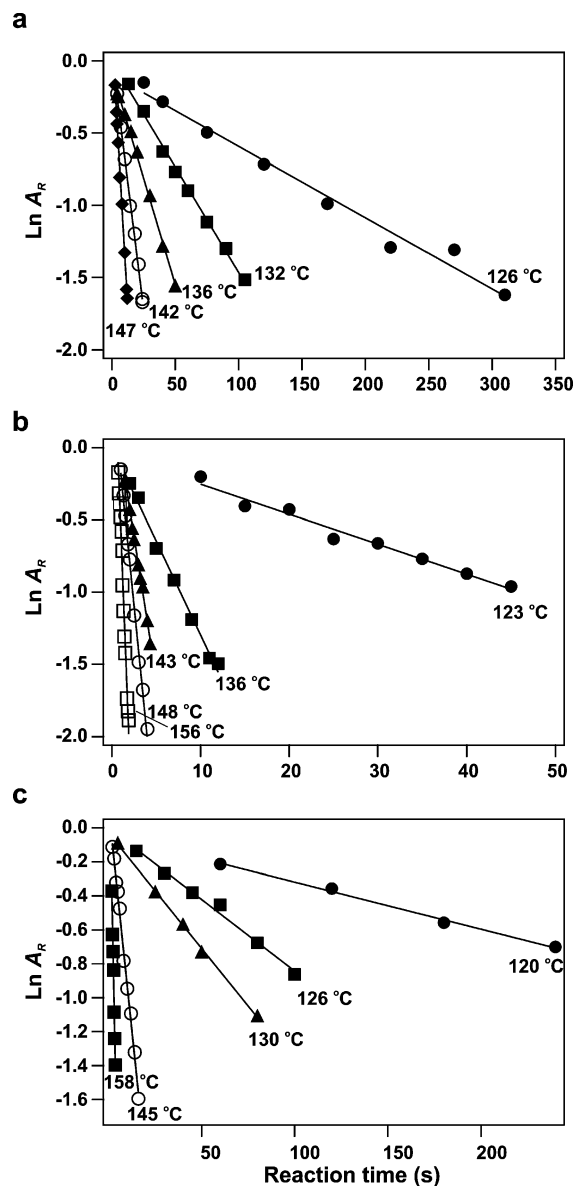
a

b

c

Figure 5. Kinetic plots obtained for the dissociation of $(scFv + \mathbf{1})^{n+/-}$ ions at charge state (a) $+7$, (b) $+12$, and (c) -8, at the temperatures shown.

in the charge state dependence of the dissociation kinetics was found for the complexes composed of the monodeoxy analogues and the scFv Ala mutants. Comparison of the Arrhenius plots for the $(scFv + L)^{n+/-}$ ions composed of $L = \mathbf{2-5}$ and the $(scFv + \mathbf{1})^{n+/-}$ ions reveals that deoxygenation *always* results in a reduction in kinetic stability (Figure 6c). This, despite the fact that deoxygenation does not always lead to a decrease in the dissociation E_a. Interestingly, no such systematic decrease in kinetic stability was found for ions composed of the scFv Ala mutants (Figure 6c). These intriguing kinetic effects are discussed in more detail below.

Despite the obvious differences in the dissociation kinetics measured for the protonated $(scFv + \mathbf{1})^{n+}$ ions at charge states $n = 6-10$, the E_a values are indistinguishable, within experimental error, with an average value of 54.4 ± 0.5 kcal/mol. Taken on its own, the similarity in the E_a values suggests identical intermolecular interactions at charge states $n = 6-10$. A decrease in E_a values is observed at higher charge states; the E_a values at the $+12$ and $+13$ charge states are ~ 10 kcal/mol

a

b

c
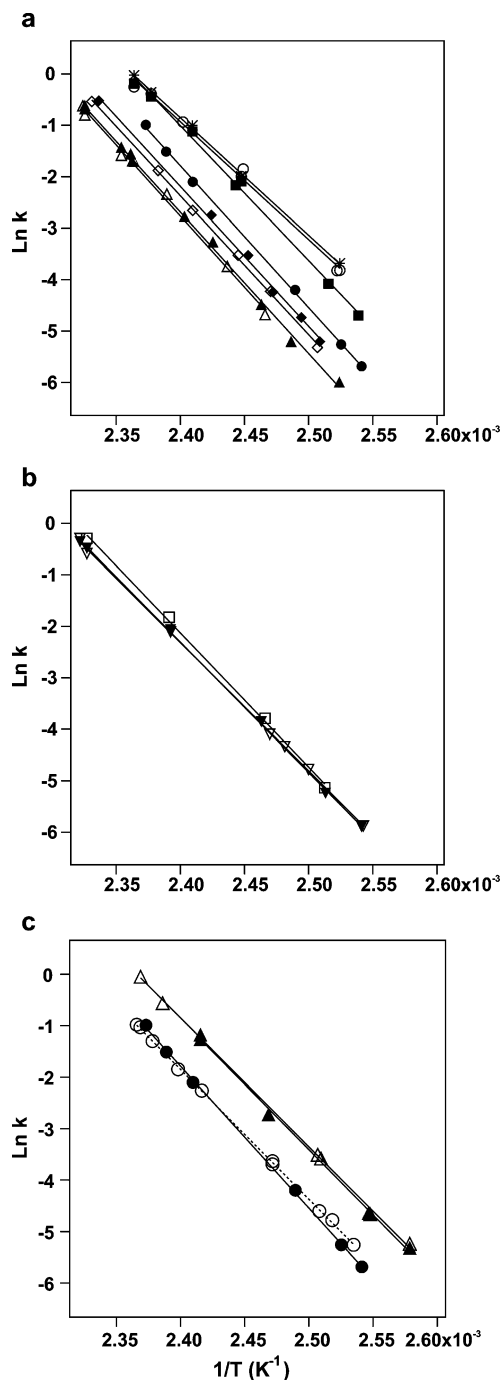
Figure 6. Arrhenius plots obtained for the loss of neutral L from the $(P + L)^{n+/-}$ ions: (a) $L = \mathbf{1}$, $P = scFv$, $+6$ (◆), $+7$ (◇), $+8$ (△), $+9$ (▲), $+10$ (●), $+11$ (■), $+12$ (○), $+13$ (×), (b) $L = \mathbf{1}$, $P = scFv$, -6 (□), -7 (▼), -8 (▽); (c) $n = +10$, $L = \mathbf{1}$, $P = scFv$ (●), $L = \mathbf{1}$, $P = His^{H101}Ala$ (○), $L = \mathbf{4}$, $P = scFv$ (▲), $L = \mathbf{4}$, $P = His^{H101}Ala$ (△).

lower than those of the lower charge states. The decrease in E_a indicates a reduction in or weakening of the intermolecular interactions between $\mathbf{1}$ and scFv, consistent with Coulombic repulsion-induced structural changes at these higher charge states. The E_a values for the deprotonated $(scFv + \mathbf{1})^{n-}$ ions, at charge states $n = 6-8$, are similar, with an average value of 50.5 ± 1.2 kcal/mol. This is ~ 4 kcal/mol smaller than the average E_a value determined for the corresponding protonated ions. The difference in E_a values indicates that the protonated and deprotonated ions are structurally distinct, although from

Table 1. Arrhenius Parameters Determined for the Dissociation Reaction: $(scFv + L)^{n+/-} \rightarrow scFv^{n+/-} + L$, where L = **1−5**[a]

ligand	charge state	E_a (kcal/mol)	$\Delta_L E_a$ (kcal/mol)	A (s^{-1})
1	−6	51.8 ± 1.3 [b]	−	$10^{26.3 \pm 0.7}$ [b]
	−7	50.3 ± 0.5	−	$10^{25.4 \pm 0.3}$
	−8	49.5 ± 0.5 [b]	−	$10^{25.0 \pm 0.3}$ [b]
	+6	54.0 ± 1.3 [b]	−	$10^{27.4 \pm 0.7}$ [b]
	+7	53.6 ± 0.7 [b]	−	$10^{27.1 \pm 0.4}$ [b]
	+8	54.9 ± 1.5 [b]	−	$10^{27.6 \pm 0.8}$ [b]
	+9	54.6 ± 0.8 [b]	−	$10^{27.5 \pm 0.4}$ [b]
	+10	54.7 ± 0.6 [b]	−	$10^{27.9 \pm 0.7}$ [b]
	+11	52.1 ± 1.4	−	$10^{26.9 \pm 0.8}$
	+12	45.6 ± 1.6	−	$10^{23.5 \pm 0.8}$
	+13	45.4 ± 0.8	−	$10^{23.4 \pm 0.4}$
2	−7	47.3 ± 1.3	3.0 ± 1.4	$10^{24.5 \pm 0.7}$
	−8	49.0 ± 1.1	0.5 ± 1.2	$10^{25.4 \pm 0.6}$
	+6	45.7 ± 0.3	8.3 ± 1.5	$10^{23.7 \pm 0.8}$
	+7	47.0 ± 1.5	6.6 ± 1.7	$10^{24.3 \pm 0.8}$
	+8	48.5 ± 0.9	6.4 ± 1.7	$10^{25.0 \pm 0.5}$
	+9	49.9 ± 0.7	4.7 ± 1.1	$10^{25.7 \pm 0.4}$
	+10	46.5 ± 0.7	8.2 ± 0.9	$10^{24.2 \pm 0.4}$
	+11	43.7 ± 1.5	8.4 ± 2.1	$10^{22.9 \pm 0.8}$
	+12	43.3 ± 1.1	2.3 ± 1.9	$10^{23.1 \pm 0.6}$
	+13	41.8 ± 1.3	3.6 ± 1.5	$10^{22.3 \pm 0.7}$
3	−7	48.4 ± 0.5	1.9 ± 0.7	$10^{25.1 \pm 0.3}$
	−8	48.1 ± 0.7	1.4 ± 0.9	$10^{25.0 \pm 0.4}$
	+6	48.1 ± 0.6	5.9 ± 1.4	$10^{24.7 \pm 0.3}$
	+7	48.0 ± 0.6	5.6 ± 0.9	$10^{24.6 \pm 0.3}$
	+8	47.6 ± 0.2	7.3 ± 1.5	$10^{24.2 \pm 0.1}$
	+9	47.7 ± 0.6	6.9 ± 1.0	$10^{24.3 \pm 0.3}$
	+10	48.5 ± 0.9	6.2 ± 1.1	$10^{25.0 \pm 0.5}$
	+11	41.0 ± 1.0	11.1 ± 1.7	$10^{21.3 \pm 0.6}$
	+12	39.4 ± 1.0	6.2 ± 1.9	$10^{20.7 \pm 0.6}$
	+13	37.0 ± 0.7	8.4 ± 1.1	$10^{19.4 \pm 0.4}$
4	−7	45.6 ± 1.3	4.7 ± 1.4	$10^{23.5 \pm 0.7}$
	−8	45.0 ± 0.5 [b]	4.5 ± 0.7	$10^{23.2 \pm 0.3}$ [b]
	+6	48.1 ± 0.8 [b]	5.9 ± 1.5	$10^{24.8 \pm 0.4}$ [b]
	+7	50.3 ± 1.3 [b]	3.3 ± 1.5	$10^{25.8 \pm 0.7}$ [b]
	+8	51.7 ± 0.9 [b]	3.2 ± 1.7	$10^{26.4 \pm 0.5}$ [b]
	+9	52.3 ± 1.2 [b]	2.4 ± 1.4	$10^{26.7 \pm 0.7}$ [b]
	+10	49.9 ± 1.0 [b]	4.8 ± 1.2	$10^{25.8 \pm 0.6}$ [b]
	+11	48.2 ± 1.2	3.9 ± 1.8	$10^{25.2 \pm 0.7}$
	+12	46.1 ± 1.3	−0.5 ± 2.1	$10^{24.4 \pm 0.7}$
	+13	46.8 ± 1.0	−1.4 ± 1.3	$10^{24.8 \pm 0.6}$
5	−7	50.1 ± 0.8	0.2 ± 0.9	$10^{26.2 \pm 0.4}$
	−8	49.0 ± 1.3	0.5 ± 1.4	$10^{25.5 \pm 0.7}$
	+6	45.5 ± 1.1	8.5 ± 1.7	$10^{23.6 \pm 0.6}$
	+7	45.5 ± 0.9	8.1 ± 1.1	$10^{23.6 \pm 0.5}$
	+8	46.9 ± 1.5	8.0 ± 2.1	$10^{24.4 \pm 0.8}$
	+9	47.5 ± 0.8	7.1 ± 1.1	$10^{24.6 \pm 0.4}$
	+10	46.1 ± 0.8	8.6 ± 1.0	$10^{24.0 \pm 0.4}$
	+11	45.6 ± 0.9	6.5 ± 1.7	$10^{24.1 \pm 0.5}$
	+12	45.3 ± 1.1	0.3 ± 1.9	$10^{24.3 \pm 0.6}$
	+13	44.3 ± 0.8	1.1 ± 1.1	$10^{23.9 \pm 0.5}$

[a] Errors are one standard deviation. [b] Values taken from ref 13b.

these data alone the nature of the structural differences cannot be elucidated. The structural differences presumably arise from differences in the residues that are charged in the protonated and deprotonated ions and, possibly, differences in charge solvation. While the location of the charges sites cannot be ascertained, in the absence of Coulombic repulsion effects or differential charge solvation, the most acidic (Asp and Glu) or basic (Arg, His, Lys) residues represent the thermodynamically favored sites of charging. Interestingly, inspection of the crystal structure of the (scFv + **1**) complex reveals that the acidic residues are remote from the ligand binding site, whereas there are a number of strongly basic residues located in and around the binding site. Consequently, charge-induced structural effects might be expected to be most significant in the case of the protonated ions.

The A-factors for the dissociation of the $(scFv + 1)^{n+/-}$ ions and the ions of the modified complexes range from 10^{20} to 10^{28} s^{-1}. These values translate to entropies of activation ($\Delta S^{\ddagger}$) of 30 to 68 cal mol^{-1} K^{-1} at 415 K.[29] The A-factors measured for the modified complexes fall in this same range. Notably, the magnitude of the A-factors exhibits a degree of correlation with the magnitude of the E_a values. The origin of large A-factors, $>10^{20}$ s^{-1}, which are typical for the dissociation of large noncovalent complexes,[13,14,16,30] and their correlation with E_a remains a matter of debate. Our laboratory has previously suggested that the large A-factors reflect, in part, the softening of numerous vibrational modes that occurs upon the dissociation of the intermolecular interactions that stabilize the complexes.[13a] Additionally, changes in the conformational flexibility of the protein and ligand during dissociation can contribute to the A-factors, *vide infra*.

Intermolecular Interactions Stabilizing the $(scFv + 1)^{n+/-}$ Ions. Stabilizing Role of Ligand OH Groups. The stabilizing role of individual ligand OH groups was evaluated from the difference in E_a values ($\Delta_L E_a$) determined for the $(scFv + 1)^{n+/-}$ ions and the corresponding $(scFv + L)^{n+/-}$ ions containing one of the monodeoxy analogues (L = **2−5**). The $\Delta_L E_a$ values, calculated using eq 4, are listed in Table 1.

$$\Delta_L E_a = E_a(scFv + \mathbf{1})^{n+/-} - E_a(scFv + L)^{n+/-} \qquad (4)$$

Deoxygenation of **1** at Gal C3 and C6 results in a measurable decrease in the dissociation E_a for the protonated ions at all charge states investigated. The $\Delta_L E_a$ values for Gal C3 and C6 OH range from 2 to 8 and 6 to 11 kcal/mol, respectively. Similarly, deoxygenation of **1** at Man C4 and C6 results in a measurable decrease in E_a at charge states $n \leq 11$. The $\Delta_L E_a$ values for Man C4 and C6 OH range from 2 to 6 and 7 to 9 kcal/mol, respectively. At $n = 12$ and 13, the $\Delta_L E_a$ values are ~ 0 kcal/mol and are suggestive of charge-induced structural changes of the binding site. Taken together, these results imply that each of the four OH groups investigated can contribute to stabilizing the gaseous $(scFv + \mathbf{1})^{n+}$ ions, although the strength and, perhaps, the nature of interaction is charge state dependent.

The role of ligand OH groups in stabilizing the complex is significantly different in the case of the deprotonated ions. Of the OH groups investigated, only the Man C4 OH group engages in a reasonably strong (~5 kcal/mol) intermolecular interaction within the $(scFv + \mathbf{1})^{n-}$ ions at charge states −7 and −8. The Gal C3 and C6 OH groups may also participate in stabilizing the complex at these charge states. But these interactions, if present, are relatively weak, ≤3 kcal/mol.

Stabilizing Role of scFv Amino Acid Residues. The role of specific amino acid residues in stabilizing the gaseous $(scFv + \mathbf{1})^{n+/-}$ ions was evaluated using an alanine scanning approach. The residues chosen for mutation were selected based on consideration of the intermolecular H-bonds identified in the crystal structure and from interactions suggested from the MD simulations performed on the $(scFv + \mathbf{1})^{8+/-}$ ions, *vide infra*. Listed in Table 2 are values of $\Delta_P E_a$ calculated for the protonated and deprotonated ions using eq 5. Because of the limited

(29) Steinfeld, J. I. *Chemical kinetics and dynamics*; Prentice Hall, Inc.: Upper Saddle River, NJ, 1999.
(30) Wang, W. J.; Kitova, E. N.; Sun, J. X.; Klassen, J. S. *J. Am. Soc. Mass Spectrom.* **2005**, *16*, 1583−1594.

Table 2. Arrhenius Parameters Determined for the Dissociation of (scFv + L)$^{n+/-}$ Ions Composed of the Trisaccharide Ligands, L = **1**–**5**, and scFv Mutants[a]

mutant	ligand	n	E_a (kcal/mol)	$\Delta_P E_a$ (kcal/mol)	$\Delta_{PL} E_a$ (kcal/mol)	A (s^{-1})
His^{101H}Ala	**1**	+6	49.1 ± 0.6[b]	4.9 ± 1.4	–	10$^{25.1\pm0.3}$[b]
	1	+7	49.9 ± 0.5[b]	3.7 ± 0.9	–	10$^{25.1\pm0.3}$[b]
	1	+8	52.1 ± 1.0[b]	2.8 ± 1.8	–	10$^{26.2\pm0.5}$[b]
	1	+9	49.9 ± 1.5[b]	4.7 ± 1.7	–	10$^{25.1\pm0.8}$[b]
	1	+10	50.0 ± 0.3[b]	4.7 ± 0.7	–	10$^{25.5\pm0.2}$[b]
	1	−8	47.1 ± 0.8	2.4 ± 0.9	–	10$^{24.0\pm0.4}$
	4	+6	50.1 ± 1.4[b]	–	3.9 ± 1.9	10$^{25.7\pm0.7}$[b]
	4	+7	51.0 ± 1.3[b]	–	2.6 ± 1.5	10$^{26.2\pm0.7}$[b]
	4	+8	52.0 ± 0.6[b]	–	2.9 ± 1.6	10$^{26.6\pm0.3}$[b]
	4	+9	51.9 ± 0.6[b]	–	2.7 ± 1.0	10$^{26.5\pm0.3}$[b]
	4	+10	49.4 ± 0.8[b]	–	5.3 ± 1.0	10$^{25.4\pm0.4}$[b]
	4	−8	45.2 ± 0.7	–	4.3 ± 0.9	10$^{23.4\pm0.4}$
His^{101H}Arg	**1**	+10	51.5 ± 0.04	3.2 ± 0.6	–	10$^{26.1\pm0.02}$
His^{101H}Lys	**1**	+10	51.5 ± 1.3	3.2 ± 1.4	–	10$^{26.1\pm0.7}$
	4	+10	49.4 ± 0.8	–	5.3 ± 1.0	10$^{25.4\pm0.4}$
His^{101H}Gln	**1**	+10	51.4 ± 0.6	3.3 ± 0.8	–	10$^{26.1\pm0.3}$
	4	+10	49.8 ± 2.2	–	4.9 ± 2.3	10$^{25.7\pm1.2}$
His^{34L}Ala	**1**	+7	49.3 ± 0.3	4.3 ± 0.8	–	10$^{24.8\pm0.2}$
	1	+8	50.9 ± 0.4	4.0 ± 1.6	–	10$^{25.5\pm0.2}$
	1	+9	49.7 ± 0.3	4.9 ± 0.9	–	10$^{24.9\pm0.2}$
	1	+10	50.7 ± 0.7	4.0 ± 0.9	–	10$^{25.5\pm0.4}$
	1	−8	49.7 ± 1.0	−0.2 ± 1.1	–	10$^{24.9\pm0.5}$
	2	+6	46.2 ± 1.7	–	7.8 ± 2.1	10$^{24.0\pm1.0}$
	2	+7	47.6 ± 1.3	–	6.0 ± 1.5	10$^{24.6\pm0.7}$
	2	+8	47.2 ± 1.0	–	7.7 ± 1.8	10$^{24.3\pm0.5}$
	2	+9	49.0 ± 1.7	–	5.6 ± 1.9	10$^{25.2\pm0.9}$
	2	+10	45.8 ± 1.3	–	8.9 ± 1.4	10$^{23.7\pm0.7}$
	2	−8	45.6 ± 1.0	–	3.9 ± 1.1	10$^{23.4\pm0.5}$
Asn^{96L}Ala	**1**	+6	50.7 ± 0.5	3.3 ± 1.4	–	10$^{25.6\pm0.3}$
	1	+7	50.5 ± 0.8	3.1 ± 1.1	–	10$^{25.4\pm0.4}$
	1	+8	52.6 ± 0.6	2.3 ± 1.6	–	10$^{26.4\pm0.4}$
	1	+9	53.2 ± 0.6	1.4 ± 1.0	–	10$^{26.8\pm0.3}$
	1	+10	51.1 ± 1.1	3.6 ± 1.3	–	10$^{25.9\pm0.6}$
	1	−8	51.2 ± 0.8	−1.7 ± 0.9	–	10$^{25.6\pm0.4}$
	3	+8	49.2 ± 0.6	–	5.7 ± 1.6	10$^{24.2\pm0.3}$
	3	+9	47.8 ± 0.5	–	4.9 ± 0.9	10$^{24.2\pm0.3}$
	3	+10	46.9 ± 0.8	–	7.8 ± 1.0	10$^{24.1\pm0.4}$
	3	−8	48.1 ± 0.8	–	1.4 ± 0.9	10$^{25.0\pm0.4}$
His^{35L}Ala	**1**	+8	47.5 ± 1.1	7.4 ± 1.9	–	10$^{23.9\pm0.6}$
	1	+9	51.0 ± 1.0	3.6 ± 1.3	–	10$^{25.7\pm0.5}$
	1	+10	47.9 ± 0.9	6.8 ± 1.1	–	10$^{24.2\pm0.5}$
	1	−8	48.3 ± 0.5	1.2 ± 0.9	–	10$^{24.6\pm0.3}$
His^{97L}Ala	**1**	+7	49.4 ± 0.6	4.2 ± 0.9	–	10$^{24.9\pm0.3}$
	1	+8	50.7 ± 1.0	4.2 ± 1.8	–	10$^{25.5\pm0.5}$
	1	+9	53.4 ± 0.5	1.2 ± 0.9	–	10$^{26.9\pm0.3}$
	1	+10	51.8 ± 0.8	2.9 ± 1.0	–	10$^{26.3\pm0.4}$
	1	−8	49.4 ± 0.3	0.1 ± 0.6	–	10$^{24.9\pm0.2}$

[a] Errors are one standard deviation. [b] Values taken from ref 13b.

availability of **1**, measurements were restricted to the +7 to +10 and −8 charge states.

$$\Delta_P E_a = E_a(\text{scFv} + \mathbf{1})^{n+/-} - E_a(\text{scFv}_{\text{mutant}} + \mathbf{1})^{n+/-} \quad (5)$$

Intermolecular interactions were positively identified at five of the scFv residues investigated: His^{101H}, His^{34L}, His^{35H}, His^{97L}, Asn^{96L}. As reported previously, the $\Delta_P E_a$ values determined for the His^{101H}Ala mutants (which range from 2 to 5 kcal/mol) indicate the presence of an interaction at charge states +6 to +10 and −8.[13b] The $\Delta_P E_a$ values determined in the present study suggest intermolecular interactions at His^{34L} (at charge states +7 to +10), His^{35L} (at charge states +8 to +10), His^{97L} (at charge states +7 to +10), and Asn^{96L} (at charge states +6 to +10). It is interesting to note that none of these four residues participate in interactions at the −8 charge state. These results are further evidence that the intermolecular interactions within

the protonated and deprotonated (scFv + **1**)$^{n+/-}$ ions are markedly different.

To evaluate the influence of other modifications of the scFv on the stability of the (scFv + **1**)$^{n+}$ ions, BIRD measurements were performed on complexes of **1** with the His^{101H}Arg, His^{101H}Lys, and His^{101H}Gln mutants at the +10 charge state. Despite the differences in the structures of the side chains, the $\Delta_P E_a$ values for these three mutants are similar, ~3 kcal/mol, Table 2. These values are ~1 kcal/mol lower than the $\Delta_P E_a$ value determined for the His^{101H}Ala mutant. These results may suggest that the side chain of each of these residues is capable of forming a weak H-bond with **1**. Replacement of His with the more basic Arg might be expected to promote protonation at the 101H position. However, the similarity in the $\Delta_P E_a$ values determined for His^{101H}Arg, His^{101H}Lys, and His^{101H}Gln suggests that this residue is neutral in all cases. These results indicate that mutation to residues other than Ala can be used to carry out the BIRD/

FGR method. The use of alternative mutations may be beneficial in cases where mutation to Ala is too extreme a modification and results in a change in higher order structure of the protein in solution.

H-Bond Donor/Acceptor Pairs within the $(scFv + 1)^{n+/-}$ Ions. As described above, it is possible to identify H-bond donor/acceptor pairs involved in stabilizing the $(scFv + 1)^{n+/-}$ ions from the magnitude of the ΔE_a values determined for specific modifications to the protein and ligand. In principle, for a given H-bond donor/acceptor pair, the $\Delta_L E_a$ and $\Delta_L E_a$ values, as well as the $\Delta_{P-L} E_a$ values, eq 6, will be indistinguishable.

$$\Delta_{P-L} E_a = E_a(scFv + 1)^{n+/-} - E_a(scFv_{mutant} + L)^{n+/-} \qquad (6)$$

It was shown previously that the values of $\Delta_L E_a$, $\Delta_P E_a$, and $\Delta_{P-L} E_a$ corresponding to modification at Man C4 OH and His[101H] are identical, within error, at charge states +6 to +10 and −8. These results were presented as evidence that Man C4 OH and His[101H] constitute a donor/acceptor pair within the $(scFv + 1)^{n+/-}$ ions.[13b] On the basis of the present results, this interaction is lost at charge states $n \geq 12$. The present results also suggest an interaction between His[34L] and Gal C3 OH at charge states +7 to +10. For this donor/acceptor pair, the average $\Delta_L E_a$ and $\Delta_{P-L} E_a$ values are indistinguishable within experimental error. However, the $\Delta_P E_a$ values are consistently smaller, by several kcal/mol. Asn[96L] and Gal C6 OH constitute another donor/acceptor pair. Again, the $\Delta_P E_a$ values are consistently smaller than the corresponding $\Delta_L E_a$ and $\Delta_{P-L} E_a$ values. At present, a definitive explanation for the absence of equivalency in the $\Delta_L E_a$, $\Delta_{P-L} E_a$, and $\Delta_P E_a$ values is lacking. However, the smaller $\Delta_P E_a$ values suggest that the Gal C3 and C6 OH groups are promiscuous and can participate in new, albeit weaker, interactions upon mutation of His[34L] and Asn[96L], respectively, to Ala. These results may indicate that one of the basic assumptions of the BIRD/FGR method, namely that mutation of residues to Ala necessarily eliminates intermolecular interactions, may not be valid in all cases. No binding partners were identified for the interactions involving the side chains of His[35L] and His[97L]. However, from an analysis of the MD simulations, Abe C4 OH was identified as a possible binding partner for His[35L].

An attractive feature of the BIRD/FGR method is that it allows intermolecular interactions to be identified and quantified. It is instructive to compare the experimental bond energies for the three H-bond donor/acceptor pairs, His[101H]/Man C4 OH, His[34L]/Gal C3 OH, and Asn[96L]/Gal C6 OH, with energies calculated for available model systems. There are two possible types of neutral H-bonds that can form between the side chain of His and the ligand OH group: the OH group can act as a proton donor or acceptor. From a recent *ab initio* study on the interaction between imidazole and water, the best available model system, the NH−O H-bond energy is 6.0 kcal/mol and the N−HO H-bond energy is 6.7 kcal/mol.[31] These calculated energies are similar to the average interaction energy, 7.0 ± 1.4 kcal/mol, determined for the His[34L]/Gal C3 OH H-bond within the protonated ions at charge states +6 to +10. This finding suggests that the donor/acceptor pair adopt a close-to-

optimal configuration for H-bonding at these charge states, although it is not possible to establish which group serves as the donor or acceptor. The calculated energies are somewhat larger than the average energy (3.6 ± 1.2 kcal/mol) determined for the His[101H]/Man C4 OH interaction at the +6 to +10 and −8 charge states.[13b] This difference may suggest that the donor/ acceptor pair is not able to adopt the optimal configuration for H-bonding because of conformational constraints imposed by the complex. According to theoretical calculations performed on the acetamide−water complex, the NH−O interaction has an energy of 5 kcal/mol and the CO−HO interaction has an energy of 6 kcal/mol.[32] These value agrees well with the average experimental value of 6.3 ± 1.0 kcal/mol obtained for the Asn[96L]/Gal C6 OH interaction at charge states +6 to +10.

Entropic Effects. An unexpected but important finding of this study is that structural modifications of a given donor/ acceptor pair within the $(scFv + 1)^{n+/-}$ ions, which are energetically equivalent (i.e., give rise to the same change in E_a), are not necessarily kinetically equivalent. This is illustrated in Figure 6c where Arrhenius plots are shown for complexes of **1** and **4** with scFv and the His[101H]Ala mutant at the +10 charge state. First, it can be seen that the dissociation kinetics for $(scFv + 1)^{+10}$ and the complex-containing His[101H]Ala mutant are similar over the temperature range investigated, despite the difference in E_a values for the two complexes. Interestingly, replacement of **1** by **4** in the complex with His[101H]Ala results in a clear shift to faster dissociation kinetics although there is no accompanying change in E_a. Similar results were obtained at charges states +6 to +10 and −8. These results reveal that protein mutation and ligand deoxygenation do not produce equivalent effects. The average difference in the dissociation rate constants for the $(His^{101H}Ala + 1)^{n+/-}$ and $(His^{101H}Ala + 4)^{n+/-}$ ions (at charges states +6 to +10 and −8) corresponds to a difference of ~2 cal/mol K in the $\Delta S^{\ddagger}$ values.[33] A possible explanation for this phenomenon is that the Man C4 OH group (in **1**) serves to rigidify the trisaccharide (which results in a decrease in vibrational entropy) in the transition state, relative to **4**. Such a decrease in vibrational entropy (in **1**) would be expected if the OH group, upon release from the H-bond with the His[101H] group, forms an internal H-bond that restricts internal rotation of the saccharide residues. Our laboratory has previously shown that the vibrational entropy associated with motion about the glycosidic linkages in oligosaccharides in the gas phase is ≥2 cal/mol K.[34] A similar argument can be made to explain the increase in rate constants observed for the $(scFv + L)^{n-}$ ions upon removal of noninteracting ligand OH groups (Gal C6 OH and Man C6 OH). The increase in rate constants correspond to increases in the $\Delta S^{\ddagger}$ values of ~3 cal/mol K. Mutation (to Ala) of individual noninteracting scFv residues can also influence the dissociation kinetics (and $\Delta S^{\ddagger}$ values). Although, based on the kinetic data described here, these effects, when present, are generally small, <1 cal/mol K.

Our results clearly demonstrate that the kinetic stabilities of gaseous protein−ligand complexes are sensitive to the modification of interacting and, in some cases, noninteracting groups. However, only the modification of interacting groups will result

(31) Scheiner, S.; Kar, T.; Pattanayak, J. *J. Am. Chem. Soc.* **2002**, *124*, 13257−13264.

(32) (a) Dixon, D. A.; Dobbs, K. D.; Valentini, J. J. *J. Phys. Chem.* **1994**, *98*, 13345−13439. (b) Rablen, P. R.; Lockman, J. W.; Jorgensen, W. L. *J. Phys. Chem. A* **1998**, *102*, 3782−3297.

(33) Kitova, E. N.; Klassen, J. S. Manuscript in preparation.

(34) Kitova, E. N.; Wang, W.; Bundle, D. R.; Klassen, J. S. *J. Am. Chem. Soc.* **2002**, *124*, 13980−13981.
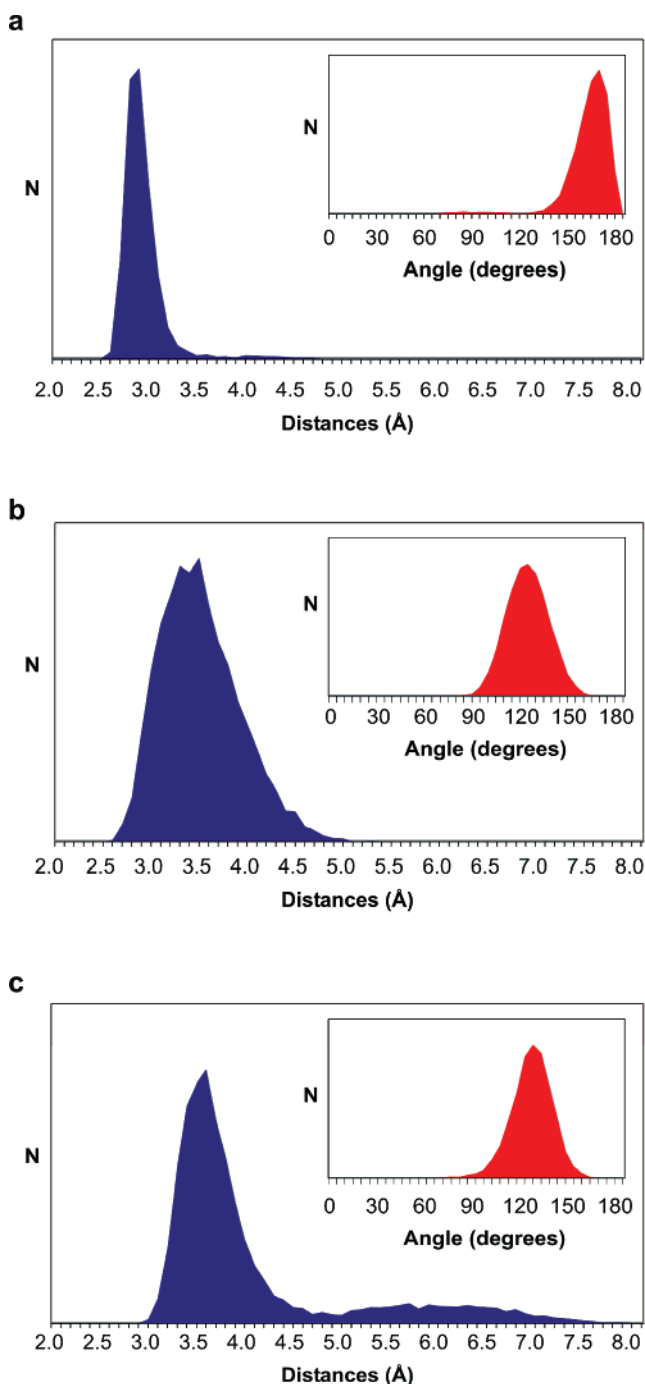
a

b

c

Figure 7. Number of occurrences (*N*) of H-bond distances, and angles (inset), obtained by MD simulations for the (a) Man C4 OH/His[101H] interaction (type 1) in the (scFv + **1**)[8+] ion; (b) Abe C4 OH/Tyr[103H] interaction (type 2) in the (scFv + **1**)[8+] ion; (c) Man C4 OH/His[101H] interaction (type 2) in the (scFv + **1**)[8−] ion.

in a change in dissociation E_a. These findings highlight the potential dangers associated with the common practice of using relative dissociation kinetics as a measure of relative E_a values.

Computational Results

A limitation of the BIRD/FGR method is the requirement that the structurally modified proteins and ligands exhibit sufficient affinity in solution to lead to detectable concentrations of complex. However, as shown in the present work, the

disruption of certain key intermolecular interactions in the (scFv + **1**) complex leads to a complete loss of binding in solution, and consequently these interactions cannot be investigated using the BIRD/FGR method. MD simulations have been used extensively to evaluate the higher order structure of gaseous ions of peptides, proteins, and other biological molecules and their noncovalent complexes.[35] Here, to assist in evaluating the structural differences between the (scFv + **1**) complex in solution and in the gas phase, MD simulations were performed on the desolvated (scFv + **1**)[n+/−] ions at charge states +8 and −8, and several structural parameters were evaluated: C_α rmsd for scFv, the OH oxygen rmsd for **1**, the dihedral angles associated with the glycosidic linkages in **1** and the intermolecular H-bonds.

Uncertainty in the location of the charges is a major challenge to the implementation of MD simulations for gaseous, multiply charged ions of macromolecules and their complexes. In the present study, ten different charge distributions were considered for the (scFv + **1**)[8+] and the (scFv + **1**)[8−] ions. Since the scFv contains eight Arg residues, Arg being the most basic amino acid in the gas phase,[24] one of the distributions involved the protonation of all eight Arg residues. Nine other distributions, in which one or more of the Arg residues were neutralized and the charge was placed instead on Lys or His residues, were also considered. Of the common amino acids, Asp and Glu have the lowest intrinsic gas phase acidities and are, in the absence of other effects, the most likely sites of deprotonation for the negatively charged (scFv + **1**)[n−] ion.[27a] Consequently, the ten charge distributions considered for the (scFv + **1**)[8−] ion involved deprotonation of Asp and Glu residues. The energies of the (scFv + **1**)[8+/−] ions, at each of the charge distributions considered, were minimized, and the lowest energy charge distributions were used for the MD simulations. A summary of the charge sites considered for the (scFv + **1**)[8+] and the (scFv + **1**)[8−] ions and the calculated energies is given as SI.

The C_α rmsd were calculated with respect to the crystal structure of the (scFv + **1**) complex.[15a] Values of 1.96 (standard deviation 0.09) and 2.77 (0.22) Å were determined for the (scFv + **1**)[8+] and (scFv + **1**)[8−] ions, respectively. Smaller C_α rmsd values were obtained when only the amino acid residues located in vicinity of the ligand binding site were considered, 0.54 (0.07) for +8 and 0.99 (0.12) Å for −8. Values of 1.77 (0.11) and 1.43 (0.18) Å were calculated for the OH oxygens in **1** at the +8 and −8 charge states, respectively. The small rmsd values, which are comparable in size to values recently reported by Patriksson and co-workers,[35e] suggest relatively minor structural changes accompanying the transfer of the complex from solution to the gas phase, at least at the +8 and −8 charge states. The average glycosidic dihedral angles in **1** [φ_1(O5[Gal]−C1[Gal]−O2[Man]−C2[Man]) and ψ_1(C1[Gal]−O2[Man]−C2[Man]−C3[Man]); φ_2(O5[Abe]−C1[Abe]−O3[Man]−C3[Man]) and ψ_2(C1[Abe]−O3[Man]−C3[Man]−C4[Man])] are for +8: $\varphi_1 = 90$ (8), $\psi_1 = 97$ (7), $\varphi_2 = 69$ (10) and $\psi_2 = 92$ (10), and for −8: $\varphi_1 = 75$ (9), $\psi_1 = 118$ (11), $\varphi_2 = 54$ (9) and $\psi_2 = 100$ (9). According to the crystal structure, these angles are $\varphi_1 = 77$, $\psi_1 = 144$, $\varphi_2 = 72$, and $\psi_2 = 104$ ($\pm 10°$). This analysis suggests that, at −8, the conformation of **1** is

(35) (a) Arteca, G. A.; Reimann, C. T.; Tapia, O. *Mass Spectrom. Rev.* **2001**, *20*, 402−422. (b) Arteca, G. A.; Tapia, O. *J. Mol. Graph. Model.* **2001**, *19*, 102−118. (c) Kaleta, D. T.; Jarrold, M. F. *J. Phys. Chem. B* **2003**, *107*, 14529−14536. (d) Kaleta, D. T.; Jarrold, M. F. *J. Phys. Chem. A* **2002**, *106*, 9655−9664. (e) Patriksson, A.; Marklund, E.; van der Spoel, D. *Biochemistry* **2007**, *46*, 933−945.

Table 3. Average Lengths (*r*), Angles (*θ*), and Occupancy (*f*) for Intermolecular H-Bonds within the (scFv + 1)$^{8+}$ and (scFv + 1)$^{8-}$ Ions Identified from MD Simulations^{a-c}
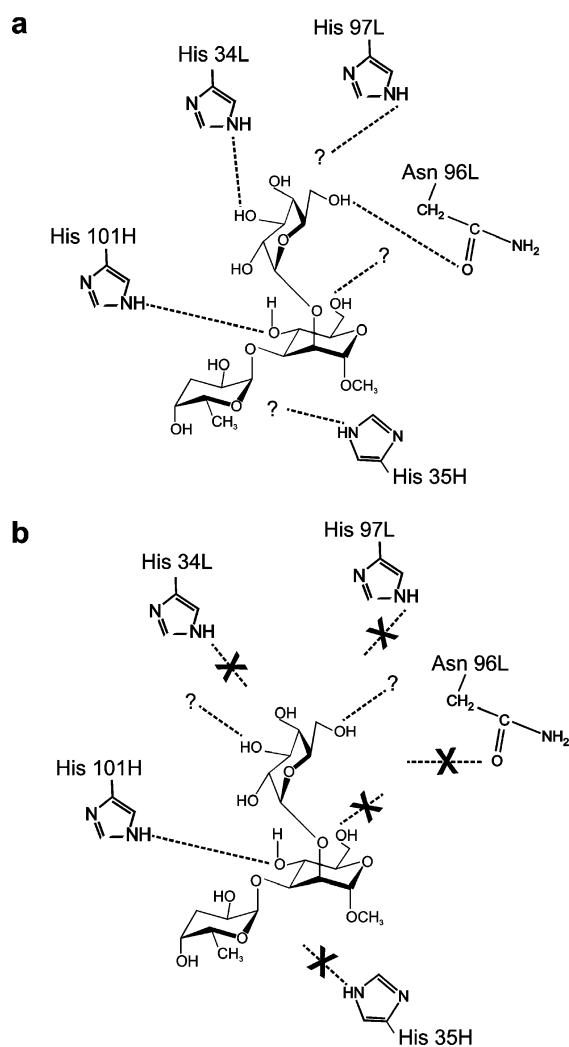
	(scFv + 1)$^{8+}$			(scFv + 1)$^{8-}$		
H-bond donor/acceptor pair	*f*	*r* (Å)	*θ* (deg)	*f*	*r* (Å)	*θ* (deg)
Trp^{98L}/Abe C4 OH	0.99	2.98 (0.16)	157.69 (9.45)	0.97	3.25 (0.22)	148.30 (10.47)
Gly^{102H}/Abe C2 OH	0.99	2.99 (0.15)	159.21 (10.51)	0.84	3.28 (0.22)	143.14 (12.67)
Trp^{93L}/Gal C4 OH	0.99	2.98 (0.16)	155.97 (10.74)		ND	
Gal C6 OH/Asn^{96L}	0.99	2.77 (0.16)	158.94 (11.02)	0.89	3.06 (0.23)	154.39 (11.93)
Man C4 OH/His^{101H}	0.96	2.86 (0.15)	162.42 (9.71)	0.44	3.54 (0.22)	130.03 (7.25)
His^{34L}/Gal C2 OH	0.72	3.02 (0.19)	146.33 (14.31)	0.94	3.24 (0.23)	158.27 (11.17)
Abe C4 OH/Tyr^{103H}	0.51	3.31 (0.32)	131.74 (8.46)		ND	
His^{35H}/Abe C4 OH	0.18	3.07 (0.18)	127.74 (6.41)	0.24	3.28 (0.24)	132.22 (10.51)
Abe C4 OH/Gly^{100H}		ND		0.92	3.26 (0.25)	153.01 (13.15)
Gal C4 OH/Asn^{95L}		ND		0.90	2.93 (0.16)	156.81 (11.81)
Trp^{93L}/Gal O(ring)		ND		0.86	3.19 (0.22)	134.30 (8.92)

^{a} The hydrogen bond distance is given with respect to the heavy atoms. ^{b} Values in parentheses correspond to one standard deviation. ^{c} ND ≡ no interaction detected.

similar to the bioactive conformation in solution. However, at +8, changes in conformation, particularly for the Gal-Man residues, are predicted.

Analysis of the MD trajectories obtained for the (scFv + **1**)$^{8+}$ and the (scFv + **1**)$^{8-}$ ions revealed two general types of intermolecular H-bonds: type 1 interactions, which exhibit a narrow distribution of bond lengths (*r*) centered at short *r* (~3 Å), a narrow distribution of bond angles (*θ*) centered at *θ* > 150° and a high occupancy (*f* > 0.90), and type 2 interactions, which exhibit a broader distribution of *r* centered at 3.1 to 3.5 Å, a broader distribution of angles, sometimes slightly bimodal in nature and centered at lower values, *θ* < 150°, and lower occupancy. Although the energies of the identified H-bonds cannot be assessed quantitatively, the characteristics of the type 1 interactions are generally associated with strong H-bonds, while the type 2 interactions correspond to weak H-bonds. The distribution of bond lengths and angles determined for the H-bond donor/acceptor pair Man C4 OH/His^{101H}, a type 1 interaction, and the Abe C4 OH/Tyr^{103H} interaction, an example of a type 2 interaction, found for the (scFv + **1**)$^{8+}$ ion are shown in Figure 7. The Man C4 OH/His^{101H} interaction persists throughout the simulation (*f* = 0.97 occupancy), and the distributions of hydrogen bond lengths and angles are narrow, with maxima close to the optimal values (2.86 Å, 162°). In contrast, the Abe C4 OH/Tyr^{103H} interaction has a much lower occupancy (*f* = 0.51), a markedly larger average *r* (3.31 Å), and a lower average *θ* (128°) values. All of the type 1 and type 2 H-bonds, along with the corresponding *r*, *θ*, and *f* values are summarized in Table 3. The corresponding the H-bond maps are shown in Figure 9.

Eight intermolecular H-bonds were identified for the (scFv + **1**)$^{8+}$ ion from the MD simulations. Of these, five are of the strong, type 1 variety: Trp^{98L}/Abe C4 OH, Gly^{102H}/Abe C2 OH, Trp^{93L}/Gal C4 OH, Gal C6 OH/Asn^{96L}, and Man C4 OH/His^{101H}. The weaker, type 2 interactions identified are His^{34L}/Gal C2 OH, Abe C4 OH/Tyr^{103H}, His^{35H}/Abe C4 OH. Nine H-bonds were identified for the (scFv + **1**)$^{8-}$ ion. Of these, only Gal C4 OH/Asn^{95L} is type 1; the remaining interactions fail to meet one or more of the criteria for a strong H-bond: Trp^{98L}/Abe C4 OH, Gly^{102H}/Abe C2 OH, Gal C6 OH/Asn^{96L}, and Man C4 OH/His^{101H}, His^{34L}/Gal C2 OH, His^{35H}/Abe C4 OH, Abe C4 OH/Gly^{100H}, and Trp^{93L}/Gal O (ring). Overall, there is a high degree of structural similarity in the (scFv + **1**)$^{8+/-}$ ions, with six common H-bonds identified. However, important differences are also evident. Notably, the weak Abe C4 OH/Tyr^{103H}

Figure 8. Interaction maps determined from BIRD/FGR data for the (scFv + **1**)$^{n+/-}$ ions at charge state (a) +8 and (b) −8.

interaction found in the (scFv + **1**)$^{8+}$ ion is replaced by a stronger Abe C4 OH/Gly^{100H} interaction in the (scFv + **1**)$^{8-}$. There are also interactions involving Gal C4 OH and Gal O (ring) which are present in the (scFv + **1**)$^{8-}$ ion but absent in the (scFv + **1**)$^{8+}$ ion. Importantly, with the exception of the His^{34L}/Gal C2 OH interaction, all of the conserved H-bonds in the (scFv + **1**)$^{8-}$ ion have larger average *r* and smaller average *θ* values than the corresponding interactions in the (scFv + **1**)$^{8-}$
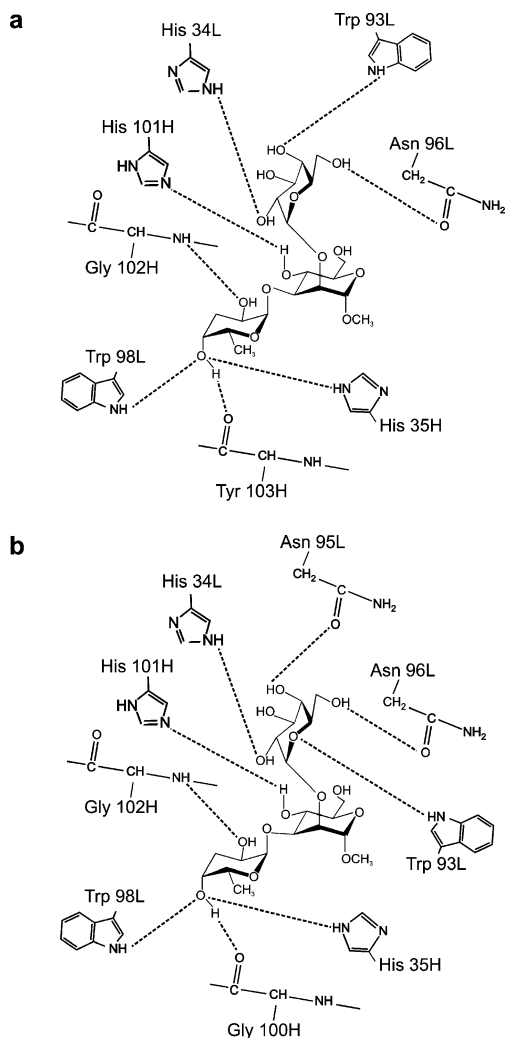
Figure 9. Interaction maps determined from MD simulations performed on the $(scFv + \mathbf{1})^{n+/-}$ ions at charge state (a) +8 and (b) −8.

ion. Also, of the three new H-bonds found in the $(scFv + \mathbf{1})^{8-}$ ion, only one of these is a type 1 interaction. Therefore, despite the greater number of interactions identified for the $(scFv + \mathbf{1})^{8-}$ ion, compared to the $(scFv + \mathbf{1})^{8+}$ ion, the individual interactions are likely weaker. Although it is not possible to draw firm conclusions regarding the relative stability of the $(scFv + \mathbf{1})^{8+/-}$ ions from the MD data, the present analysis suggests that, despite the greater number of identified interactions, the $(scFv + \mathbf{1})^{8-}$ ion is energetically less stable than the $(scFv + \mathbf{1})^{8+}$ ion. This prediction is consistent with the lower dissociation E_a determined for the $(scFv + \mathbf{1})^{8-}$ ion, compared to the $(scFv + \mathbf{1})^{+8}$ ion.

Comparison of the H-bond maps predicted by the BIRD/FGR data (Figure 8) and by the MD simulations (Figure 9) affords an opportunity to test of the predictive value of the MD simulations. For the $(scFv + \mathbf{1})^{8+}$ ion, the agreement between experiment and theory is reasonably good. Interactions between Man C4 OH and His[101H] and between Asn[96L] and Gal C6 OH were identified with both methods. An interaction between His[34L] and Gal C3 OH was predicted by BIRD/FGR; according to the simulations, His[34L] interacts with the neighboring Gal C2 OH. Also, both methods predict an interaction at His[35L], although the binding partner, Gal C4 OH, suggested by simulation could not be confirmed experimentally (because of

the unavailability of the corresponding monodeoxy analogue of **1**). The BIRD/FGR results suggest energetically important interactions involving, separately, His[97L] and Man C6 OH. According to the MD simulations, neither the amino acid residue nor the OH group engage in intermolecular H-bonds. The agreement between experiment and theory is less favorable in the case of the $(scFv + \mathbf{1})^{8-}$ ion. Of the five interactions suggested from the simulations and amenable to experimental testing (Gal C4 OH/Asn[95L], Gal C6 OH/Asn[96L], Man C4 OH/His[101H], His[34L]/Gal C2 OH, and His[35H]/Abe C4 OH), only one, the Man C4 OH/His[101H] interaction, was identified by BIRD/FGR.

On the basis of the results of the above comparison, it is concluded that the MD simulation method, as implemented in the present study, can be used to identify intermolecular interactions within noncovalent biological complexes. However, the method can lead to false positives and false negatives. These shortcomings may reflect limitations in the theoretical model, in particular deficiencies in the choice and use of fixed atomic charges and the choice of charge distributions, as well as the disparity between the computational (ns) and experimental (s) timescales. Additionally, from trajectory analysis it is not possible to quantify the H-bonds, and some of the interactions suggested computationally may not be sufficiently strong (>2 kcal/mol) to be detected using the BIRD/FGR method. Future work will focus on calculating the potential of mean force (PMF)[36] for the scFv-L interactions in the gas phase. From the PMF, the dissociation rate constants for the $(scFv + L)^{n+/-}$ ions can be computed using transition state theory.[37] This will allow for a direct comparison of the dissociation kinetics and energetics determined experimentally and predicted theoretically.

Comparison of Intermolecular Interactions Identified in the Gas Phase and in the Crystal Structure. Comparison of the intermolecular H-bond maps for the gaseous $(scFv + \mathbf{1})^{n+/-}$ ions (Figure 8) and the crystal structure of the $(scFv + \mathbf{1})$ complex (Figure 1) allows for several conclusions to be drawn. First, there is evidence for the retention of specific H-bonds: His[101H]/Man C4 OH and His[34L]/Gal C3 OH in the $(scFv + \mathbf{1})^{n+}$ ions at $n \leq 10$, and His[101H] /Man C4 OH in the $(scFv + \mathbf{1})^{n-}$ ions at $n = 7, 8$. This is an important finding, as it suggests that the structure of the binding site in the $(scFv + \mathbf{1})$ complex is at least partially conserved upon transfer of the complex from solution to the gas phase by ES. Second, nonspecific intermolecular interactions can play a significant role in stabilizing the protonated $(scFv + \mathbf{1})^{n+}$ ions. For example, the C6 OH groups of Gal and Man are found to participate in strong interactions, at least at certain charge states. According to the crystal structure of the $(scFv + \mathbf{1})$ complex, these OH groups are exposed to solvent and, according to microcalorimetry measurements, they contribute little to the binding free energy in solution.[15b] Curiously, nonspecific intermolecular interactions within the $(scFv + \mathbf{1})^{n-}$ ions were not detected. Finally, differences in intermolecular interactions identified experimentally and computationally notwithstanding, the MD data suggest that the loss of the structural water (Wat1) does not result in a dramatic change in the structure of the ligand binding site. Instead, the void created by the loss of Wat1 is filled by new intermolecular interactions between scFv and the Abe residue. Specifically,

(36) Kirkwood, J. G. *J. Chem. Phys.* **1935**, *3*, 300−313.
(37) Schenter, G. K.; Kathmann, S. M.; Garrett, B. C. *J. Chem. Phys.* **1999**, *110*, 7951−7959.

two of the three residues (His[35H], Gly[100H], and Tyr[103H]) that are suggested by the crystal structure to interact with Wat1 form new H-bonds with Abe C4 OH: His[35H]/Abe C4 OH and Abe C4 OH/Tyr[103H] interactions in the (scFv + $\mathbf{1}$)$^{8+}$ ion, and His[35H]/Abe C4 OH and Abe C4 OH/Gly[100H] interactions in the (scFv + $\mathbf{1}$)$^{8-}$ ion.

Conclusions

In summary, the first detailed and quantitative study of the intermolecular H-bonds within the protonated and deprotonated ions of a desolvated protein−ligand complex is reported. Using the BIRD/FGR method, intermolecular H-bonds stabilizing the protonated and deprotonated (scFv + $\mathbf{1}$)$^{n+/-}$ ions were identified and quantified. Three H-bond donor/acceptor pairs (His[101H]/Man C4 OH, His[34L]/Gal C3 OH, and Asn[96L]/Gal C6 OH) within the (scFv + $\mathbf{1}$)$^{n+}$ ions and one (His[101H]/Man C4 OH) within the (scFv + $\mathbf{1}$)$^{n-}$ ions were identified. The strengths of these H-bonds agree well with energies calculated for model systems. Notably, two of the interactions (His[101H]/Man C4 OH and His[34L]/Gal C3 OH) correspond to specific intermolecular H-bonds in solution. These results are compelling evidence that the binding site is, at least partially, conserved upon transfer of the (scFv + $\mathbf{1}$) complex from solution to the gas phase by ES. Additional sites of interaction on the scFv and on $\mathbf{1}$, for which the binding partner could not be elucidated, were also identified. Nonspecific intermolecular interactions, which form upon desolvation, were also identified. Importantly, the nature and strength of the intermolecular interactions can vary with charge state. In particular, it was shown that the protonated and deprotonated (scFv + $\mathbf{1}$)$^{n+/-}$ ions are structurally very different. Intermolecular H-bonds were also identified from MD simulations performed at the +8 and −8 charge states. Agreement was found for a majority of intermolecular interactions predicted from simulation and BIRD/FGR for the (scFv + $\mathbf{1}$)$^{8+}$ ion; the agreement was less favorable in the case of the (scFv + $\mathbf{1}$)$^{8-}$ ion. However, both the computational and experimental results point to structural differences for the complex at the +8 and −8 charge states. The computational results also suggest that the intermolecular interactions within the (scFv + $\mathbf{1}$)$^{-8}$ ion are inherently weaker than those found in the (scFv + $\mathbf{1}$)$^{8+}$ ion. This finding is qualitatively consistent with the lower dissociation E_a determined for the (scFv + $\mathbf{1}$)$^{8-}$ ion, compared to the (scFv + $\mathbf{1}$)$^{+8}$ ion. Finally, the MD simulations suggest that the water mediated H-bonds between the scFv and $\mathbf{1}$, which are identified in the crystal structure and are lost upon transfer of the complex from solution to the gas phase, are replaced with direct H-bonds between $\mathbf{1}$ and two of the three scFv residues originally interacting with the structural water molecule.

Supporting Information Available: Complete ref 17, Arrhenius plots (Figures S1−S3), and calculated energies for the different charge distributions for the (scFv + $\mathbf{1}$)$^{8+/-}$ ions (Tables S1 and S2). This material is available free of charge via the Internet at http://pubs.acs.org.

JA075333B